Check for updates

Geochemistry, Geophysics, Geosystems®

AGU ADVANCING EARTH AND SPACE SCIENCES

RESEARCH ARTICLE
10.1029/2024GC011462

Vortex Magnetic Domain State Behavior in the Day Plot

Wyn Williams[1], Roberto Moreno[1,2], Adrian R. Muxworthy[3,4], Greig A. Paterson[5], Lesleis Nagy[5], Lisa Tauxe[6], Ualisson Donardelli Bellon[1,7], Alison A. Cowan[3], and Idenildo Ferreira[1]

[1]School of GeoSciences, University of Edinburgh, Edinburgh, UK, [2]CONICET, Instituto de Física Enrique Gaviola (IFEG), Córdoba, Argentina, [3]Department of Earth Science and Engineering, Imperial College London, London, UK, [4]Department of Earth Sciences, University College London, London, UK, [5]Department of Earth, Ocean and Ecological Sciences, University of Liverpool, Liverpool, UK, [6]Scripps Institution of Oceanography, University of California San Diego, La Jolla, CA, USA, [7]Department of Geophysics, Institute of Astronomy, Geophysics and Atmospheric Sciences (IAG), University of São Paulo, São Paulo, Brazil

Key Points:

- Vortex domain states for magnetite predominantly have pseudo-single-domain Day plot characteristics
- If the mineralogy is known, the Day plot can provide an estimate on the dominance of stable remanence carriers

Supporting Information:

Supporting Information may be found in the online version of this article.

Correspondence to:

W. Williams,
wyn.williams@ed.ac.uk

Citation:

Williams, W., Moreno, R., Muxworthy, A. R., Paterson, G. A., Nagy, L., Tauxe, L., et al. (2024). Vortex magnetic domain state behavior in the Day plot. *Geochemistry, Geophysics, Geosystems*, *25*, e2024GC011462. https://doi.org/10.1029/2024GC011462

Received 23 JAN 2024
Accepted 31 JUL 2024

© 2024 The Author(s). Geochemistry, Geophysics, Geosystems published by Wiley Periodicals LLC on behalf of American Geophysical Union.
This is an open access article under the terms of the Creative Commons Attribution License, which permits use, distribution and reproduction in any medium, provided the original work is properly cited.

Abstract The ability of rocks to hold a reliable record of the ancient geomagnetic field depends on the structure and stability of magnetic domain-states contained within constituent particles. In paleomagnetic studies, the Day plot is an easily constructed graph of magnetic hysteresis parameters that is frequently used to estimate the likely magnetic recording stability of samples. Often samples plot in the region of the Day plot attributed to so-called pseudo-single-domain particles with little understanding of the implications for domain-states or recording fidelity. Here we use micromagnetic models to explore the hysteresis parameters of magnetite particles with idealized prolate and oblate truncated-octahedral geometries containing single domain (SD), single-vortex and occasionally multi-vortex states. We show that these domain states exhibit a well-defined trend in the Day plot that extends from the SD region well into the multi-domain region, all of which are likely to be stable remanence carriers. We suggest that although the interpretation of the Day plot and its variants might be subject to ambiguities, if the magnetic mineralogy is known, it can still provide some useful insights about paleomagnetic specimens' dominant domain state, average particle sizes and, consequently, their paleomagnetic stability.

Plain Language Summary Ancient magnetic field recordings from rocks, provide information about the early habitability of Earth and formation of the Solar System. Key to understanding the reliability of these magnetic recordings is knowing the particle size and shape of a rock's constituent magnetic minerals. Small magnetite particles ($\lessapprox$100 nm) are magnetically uniform, but as particle size increases the magnetic structures become non-uniform and increasingly complex. These different types of structures are termed domain states, and yield different magnetic hysteresis responses, often summarized on a so-called "Day" diagram—a commonly used diagnostic of domain state (or particle size). The position of particles in the size 100–1,000 nm on the Day plot is poorly quantified. This is a problem, as it has been shown in the last 5 years, that this particle size range carries the most stable magnetic recordings, lasting potentially longer than the age of the universe. These particles contain vortex-like magnetic structures. Using a numerical micromagnetic algorithm, this is the first comprehensive study to quantify the magnetic response of vortex structures on the Day plot. We show that careful use of the Day plot can provide insight into the ability of a sample to retain recordings of the ancient geomagnetic field.

1. Introduction

Knowing the domain state of magnetic minerals contained within experimental samples is central to paleo- and environmental magnetism because the domain state informs us about both the particle size and importantly the magnetic recording fidelity of its paleomagnetic signal. The "Day plot" (Day et al., 1977) is a popular way to characterize domain-states using a plot derived from magnetic hysteresis and backfield-curve measurements. Day et al. (1977) has ~3,000 citations at the time of writing. The Day plot shows the ratios of the remanent saturation magnetization normalized by saturation magnetization (M_{rs}/M_s), versus the ratio of the remanent coercivity over coercivity (B_{cr}/B_c). The smallest remanence-carrying particles, which are magnetically uniform and termed single domain (SD), have high M_{rs}/M_s and low B_{cr}/B_c and plot toward the upper left of the diagram. The largest particles (multidomain, MD) plot toward the lower right, and intermediate-sized particles (traditionally referred to as pseudo-SD or pseudo-single domain [PSD]), plot in the middle (Figure 1). Most published data fall within the

15252027, 2024, 8, Downloaded from https://agupubs.onlinelibrary.wiley.com/doi/10.1029/2024GC011462 by Test, Wiley Online Library on [07/08/2024]. See the Terms and Conditions (https://onlinelibrary.wiley.com/terms-and-conditions) on Wiley Online Library for rules of use; OA articles are governed by the applicable Creative Commons License

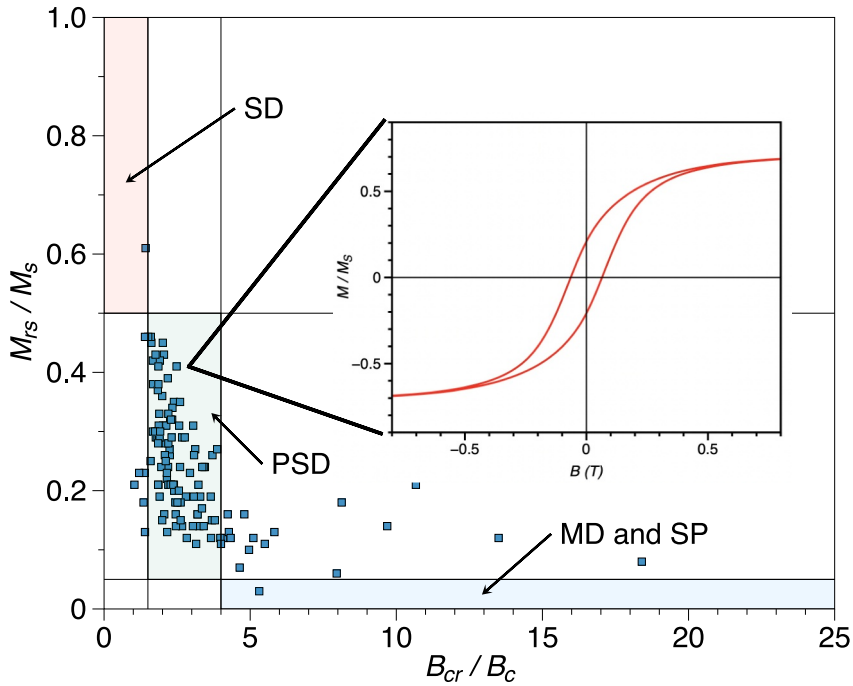


Figure 1. Hysteresis parameters from a collection of related specimens in a Day plot diagram, where the vertical axis is the remanence ratio (M_{rs}/M_s) and the horizontal axis is the coercivity ratio (B_{cr}/B_c). The inset is a typical hysteresis loop from which the ratios were derived, where the red line is the measured loop corrected for para/diamagnetic contributions. The fields single domain, pseudo-single domain, multidomain, and superparamagnetic indicate the "usual" domain structure interpretation for the respective regions of the diagram. The data are from Paterson et al. (2017).

PSD region of the Day plot, which has led several authors to criticize the use of such a plot to diagnose domain state (Roberts et al., 2018, 2019; Tauxe et al., 2002). This criticism is based partially on our general lack of understanding of what type of magnetic particles and phenomena contribute to the PSD region. Because magnetic hysteresis and backfield-curve measurements are performed on macroscopic bulk samples, the achieved magnetic parameters are a response to an assemblage of particles. These assemblages are likely not uniform in terms of domain states. For example, they can be mixtures of pure SD and MD particles that might plot within the PSD region (as do vortex states) (Dunlop, 2002b). Furthermore, mixtures of SD and superparamagnetic particles (referred to as SP, a behavior attributed to particles with instantaneous relaxation times) also plot within the PSD region (Dunlop & Carter-Stiglitz, 2006; Tauxe et al., 1996). Despite the ambiguity in its interpretation, the Day plot remains popular partly because unlike other more complex domain state diagnostic tests (e.g., Roberts et al., 2000), its related data are relatively quick and easy to measure, it attempts to identify remanence rather than induced domain states, and it is also possible to summarize results for hundreds of specimens on a single diagram.

The original domain state boundaries on the Day plot are based on a mixture of theory (Stoner & Wohlfarth, 1948) and experimental observations on synthetic (titano)magnetite samples. Significant improvements to the interpretation of Day plots were made by the theoretical analysis of Dunlop (2002a), and established trend-lines for mixtures of MD, SD, and SP domain states, and suggesting that samples plotting in the PSD region might be explained by such mixtures. While it is possible to analytically calculate the behavior of SD particles controlled by various magnetic anisotropy types, and also to experimentally determine Day plot parameters for large, individual MD crystals, understanding the behavior in the paleomagnetically important high-remanence PSD range, that is, 100–10,000 nm, has proven more challenging. There are two reasons for this: (a) production of non-interacting experimental samples with narrow particle-size distributions, which are also "stress-free" is challenging (King & Williams, 2000; Krása et al., 2011), and (b) the magnetic behavior of PSD particles is complex and theoretical models require numerical solutions (Brown, 1963).

Over the last 30 years, micromagnetics combined with nanometric magnetic imaging (Almeida et al., 2014; Harrison et al., 2002), has revolutionized our understanding of PSD particles. We now know that PSD particles

15252027, 2024, 8, Downloaded from https://agupubs.onlinelibrary.wiley.com/doi/10.1029/2024GC011462 by Test, Wiley Online Library on [07/08/2024]. See the Terms and Conditions (https://onlinelibrary.wiley.com/terms-and-conditions) on Wiley Online Library for rules of use; OA articles are governed by the applicable Creative Commons License

are dominated by single-vortex (SV) and multi-vortex (MV) structures, which have been shown (Nagy et al., 2017; Nagy, Williams, Tauxe, Muxworthy, et al., 2019) to have magnetic stabilites equal to or exceeding that of SD particles and thus challenging the long-held view that SD particles carry the most stable paleomagnetic remanence (Néel, 1949). For many magnetically soft minerals, such as magnetite, the particle size range for vortex states is predicted to be at least an order of magnitude greater than that of SD particles (Nagy et al., 2017) and thus there is an urgent need to be able to identify not only SD particles but also PSD/vortex behavior in the Day plot. In this paper, we follow Roberts et al. (2017) and refer to PSD signals as vortex signals.

1.1. How Are Vortex Domain States Represented on the Day Plot?

There have been several previous attempts to characterize the vortex state contribution to the Day plot using micromagnetic numerical models. However, these are either older studies in which approximations were made and the models do not meet modern standards such as adequate model resolution or accounting for realistic particle morphologies (Muxworthy et al., 2003; Tauxe et al., 2002; Williams & Dunlop, 1995) or the Day plot was not the main focus and the results were not comprehensive (Lascu et al., 2018; Nikolaisen et al., 2020; Valdez-Grijalva et al., 2018, 2020). Although not comprehensive, these studies have demonstrated that the Day plot is sensitive to both the particle size and morphology of vortex state particles, and that particles just larger than the SD threshold size can plot close to the MD region (Lascu et al., 2018; Valdez-Grijalva et al., 2018, 2020). Of particular note is the study of Nikolaisen et al. (2020), who examined a range of realistic particle sizes and shapes and reported predictions of SD and vortex states that are generally well grouped on the Day plot. These theoretical studies are supported by electron-beam lithography observations on samples of magnetite mono-dispersions, which observe particles in the vortex domain state size range that plot at the PSD/MD boundary in the Day plot (Krása et al., 2011). EBL samples are arrays of nearly identical crystals, which is ideal for characterizing vortex state behavior. However, the samples can suffer from stress induced by the coupling of the crystals with the thin-film substrate which, in turn, affects their hysteresis characteristics.

Therefore, there is a need to determine the vortex state contribution to the frequently used Day plot. In this paper, we have used MERRILL (Ó Conbhuí et al., 2018) to systematically determine the Day plot response for magnetite crystals as a function of both size and elongation. For that, we use distributions of randomly orientated particles that simulate mono-dispersions that are capable of displaying both SD and vortex-state behaviors.

2. Methods

Our numerical models of Day plot parameterization of hysteresis observations were obtained using the open-source software package MERRILL, version 1.8.6p (Ó Conbhuí et al., 2018; Williams, Fabian, et al., 2024), which is a three-dimensional finite-element micromagnetic modeling application. While recognizing that hysteresis parameters may depend on slight changes in particle morphology and surface irregularities, our aim is to examine hysteresis parameter trends as a function of particle size and idealized shape. We therefore consider truncated-octahedron shaped particles that were either elongated or compressed along the x-axis to create prolate or oblate particle morphologies. In some respects, this mirrors the standard single-domain analysis in ellipsoidal particles, but here we take a typical crystal morphology and allow the magnetization to occupy non-uniform magnetic domain states and non-coherent domain switching mechanisms. MERRILL requires particle geometries to be defined in terms of a finite element mesh, which were generated using the proprietary meshing package Coreform Trelis (Coreform LLC, 2017). In micromagnetic modeling it is important to have the maximum mesh size no greater than the material's exchange length l_{ex} (Rave et al., 1998), which for magnetite at 20°C takes a value of 9 nm. l_{ex} is related to the width of transitions between domains, and if it is too large the inhomogeneously magnetized states will be poorly characterized. All our model geometries were meshed at a mean size of 8 nm.

All models were of stoichiometric magnetite at 20°C defined in terms of the four temperature dependent material constants of saturation magnetization M_S, magnetocrystalline anisotropy constants K_1 and K_2, and the exchange constant A_{ex}, which have values of 4.825×10^5 A/m^2 (Pauthenet & Bochirol, 1951), -1.304×10^4 J/m^3 and -3.154×10^3 J/m^3 (Fletcher & O'Reilly, 1974) and 1.344×10^{-11} J/m (Heider & Williams, 1988), respectively. It should be noted that the models presented here do not include thermal fluctuations, whose principal effect is to reduce the remanent magnetization for weakly stable domain states. Such particles are also commonly referred to as SP particles.

15252027, 2024, 8, Downloaded from https://agupubs.onlinelibrary.wiley.com/doi/10.1029/2024GC011462 by Test, Wiley Online Library on [07/08/2024]. See the Terms and Conditions (https://onlinelibrary.wiley.com/terms-and-conditions) on Wiley Online Library for rules of use; OA articles are governed by the applicable Creative Commons License

A total of 556 models of prolate and oblate geometries were obtained, covering a wide range of stable-single-domain (SSD, hereafter referred to as SD) and single-vortex (SV) domain states. The prolate geometries consist of 17 particle sizes from 40 to 200 nm in 10 nm steps. Each size has elongations along ⟨100⟩ with axial ratios (AR, long axis/short axis) of 1.00–2.00 in 0.05 steps, 2.00 to 3.00 in 0.25 steps, and 3.00 to 5.00 in 1.00 steps. Oblate particles have 16 sizes from 45 to 195 nm in steps of 10 nm, and each size is compressed along ⟨100⟩ to ARs of 0.909, 0.500, 0.250, and 0.167. All particle sizes are quoted as equivalent spherical volume diameters (ESVD). A further set of models were calculated for a three-dimensional cruciform shape consisting of three mutually perpendicular parallelepiped limbs intersecting each other at their center, where each parallelepiped has a relative dimension of $1 \times 1 \times 7$, similar to that reported by Tauxe et al. (2002). Seventeen such models were made for ESVD particle sizes of 40–200 nm in 10 nm steps.

M_{rs}, B_c, and B_{cr} were obtained from simulated first-order reversal curves, described by Nagy, Moreno, Muxworthy, et al. (2024) using peak fields of 200 mT and maximum field steps of 4 mT. Hysteresis loops were calculated by first saturating the magnetization in the direction of the applied field. Thereafter, the initial guess at each field step was the local energy minimum magnetic domain structure solution of the previous field step. For each particle, we use an average of 29 different field directions from a Fibonacci distribution (Hannay & Nye, 2004) over an octant of the sphere between azimuthal angles $\phi = 0, \pi/2$ and polar angle $\theta = 0, \pi/2$ symmetric to the particle elongation along ⟨100⟩. Back-field curves, again at 4 mT increments, were generated for the 29 different field directions and averaged before extracting M_{rs}, B_c, and B_{cr} for each particle size and morphology.

3. Results

Almost all domain states modeled here with ESVD particle sizes between 40 and 200 nm are either SD or SV, but within these primary types of states, the magnetization can align along the easy or hard magnetocrystalline directions, or along the short or long particle shape axes. Example domain states are shown in Figure 2. We see that prolate particles (Figures 2a–2c) have their magnetization and vortex cores aligned along the easy shape (long) axis, but as particle size grows, the vortex core shape and orientation can distort, for example, Figure 2c. Particles with sizes close to the critical SD particle size, d_c, will gradually change their domain state from SD to SV, becoming less uniform by exhibiting "flowering" of the magnetization at the particle surface, for example, Figure 2e (Williams & Dunlop, 1990), where the domain state classification is not clear. Larger SD oblate particles form "S" states within the oblate plane for example, Figure 2h (Zhao et al., 2014). Occasionally, 200 nm oblate particles form MV states, for example, Figure 2i. Each of these slight variations influences the resulting M_{rs}/M_s and B_{cr}/B_c values.

Each modeled mono-dispersion consists of 29 particles whose domain states are frequently of the same type, but variations may occur due to the different applied field directions. This is more common for particle sizes close to d_c, where some particles will nucleate SV states while others remain in the SD state. For the largest particle sizes, almost all are in the SV state, but vortex core curvature can be present. In our models, some domain structures such as the "S" state are found only in oblate particle morphologies. The MV domain state is only found in particles with AR = 0.25, and only for 18 of the 29 particles in our mono-dispersion.

Predicted Day plot parameters for ellipsoidal magnetite are shown in Figure 3, with a close-up on a linear horizontal axis shown in Figure S1 in Supporting Information S1. These predominantly SD and SV particles often plot outside the M_{rs}/M_s and B_{cr}/B_c limits for SD and PSD particles, but nevertheless fall within a well-defined diagonal band across the (log-log) Day plot. Results for cruciform models are only included in the enlarged section in Figure 4.

3.1. SD Particle Behavior on the Day Plot

Regardless of particle morphology, only SD or near-SD states should exist above $M_{rs}/M_s = 0.5$. In this study we take SD states to include different degrees of flowering and "S-type" states; "S-type" states are treated as SD as they do not contain a vortex core (see Figure 2h), although in some cases these will have values of M_{rs}/M_s less than 0.5. In general, M_{rs}/M_s values of random distributions of SD particles are controlled by their magnetic anisotropy, either crystalline or particle shape, or a combination of the two (e.g., Dunlop & Özdemir, 1997). For mono-dispersions of SD particles we expect our models to agree with analytic calculations for M_{rs}/M_s that are easily determined using:

15252027, 2024, 8, Downloaded from https://agupubs.onlinelibrary.wiley.com/doi/10.1029/2024GC011462 by Test, Wiley Online Library on [07/08/2024]. See the Terms and Conditions (https://onlinelibrary.wiley.com/terms-and-conditions) on Wiley Online Library for rules of use; OA articles are governed by the applicable Creative Commons License

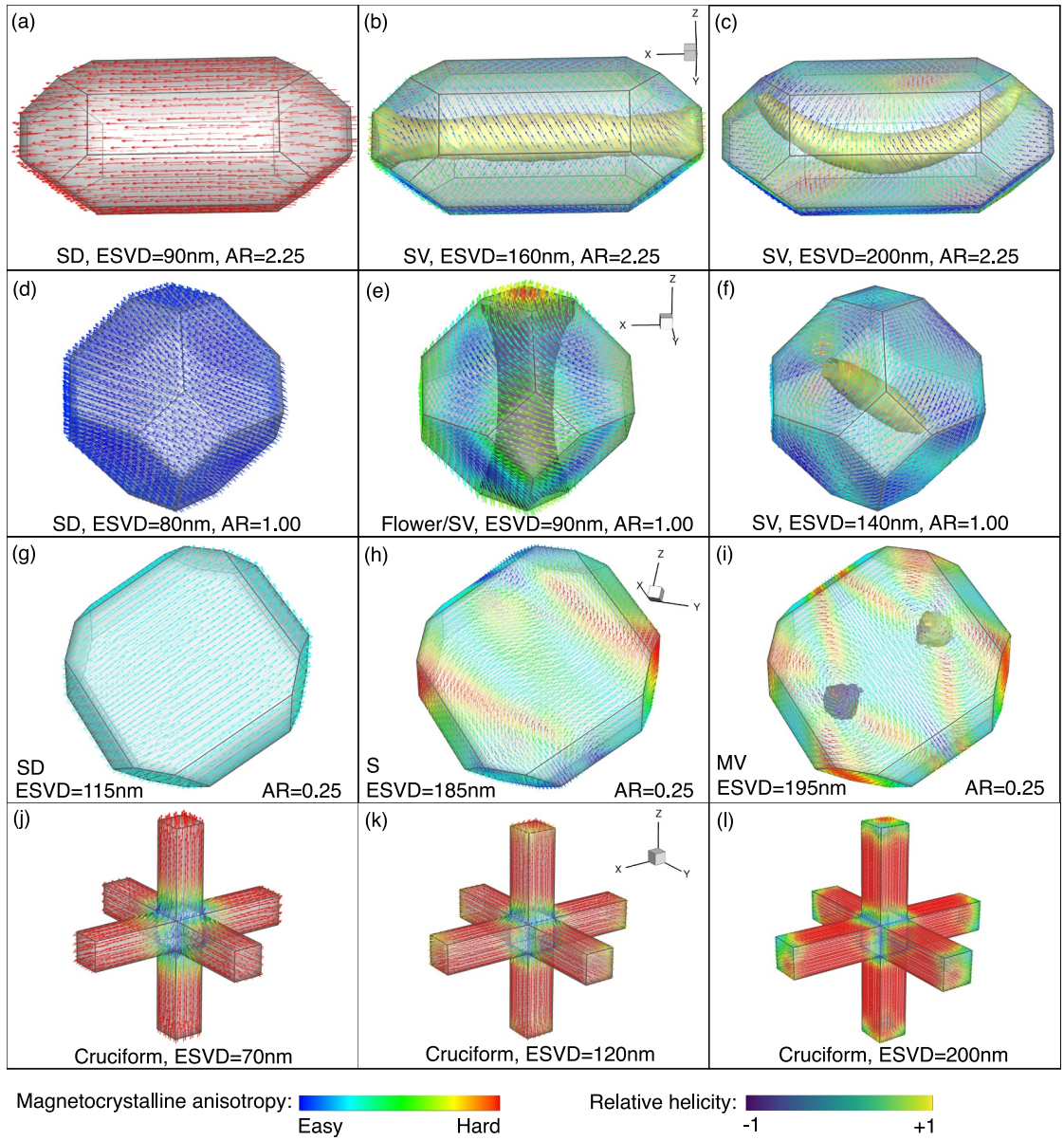


Figure 2. A selection of typical domain states that are nucleated as a function of particle size (equivalent spherical volume diameters) and shape (axial ratios). Particle orientation within each row is the same and indicated by the axes in the center panel where x, y, and z are along [100], [010], and [001], respectively. The magnetic structures are shown as surface vectors, colored according to alignment with the cubic magnetocrystalline anisotropy. Where vortex structures nucleate within a particle, its helicity isosurface is shown at ±95% of its maximum value. Each truncated-octahedral particle domain state is labeled as single-domain (SD), single-vortex, S-state, or multi-vortex. Domain states in cruciform particles are SD-like within each limb.

$$M_{rs}/M_s = \int_{\theta_{min}}^{\theta_{max}} \int_{\phi_{min}}^{\phi_{max}} \hat{\mathbf{m}} \cdot \hat{\mathbf{h}}, \quad (1)$$

where ϕ and θ are the spherical coordinate azimuth and polar angle respectively. M_{rs}/M_s will decrease with the number of dominant anisotropy axes as shown in Table 1.

Experimental observations of SD particles with $M_{rs}/M_s < 0.5$ indicate the presence of significant magnetic particle interactions (Muxworthy et al., 2003), and/or a particle size distribution that exceeds the narrow SD particle size range, and/or a particle size distribution that includes significant SP particles (Tauxe et al., 1996). For our modeled mono-dispersions, an enlarged section of the Day plot (Figure 4) shows three groupings of M_{rs}/M_s values

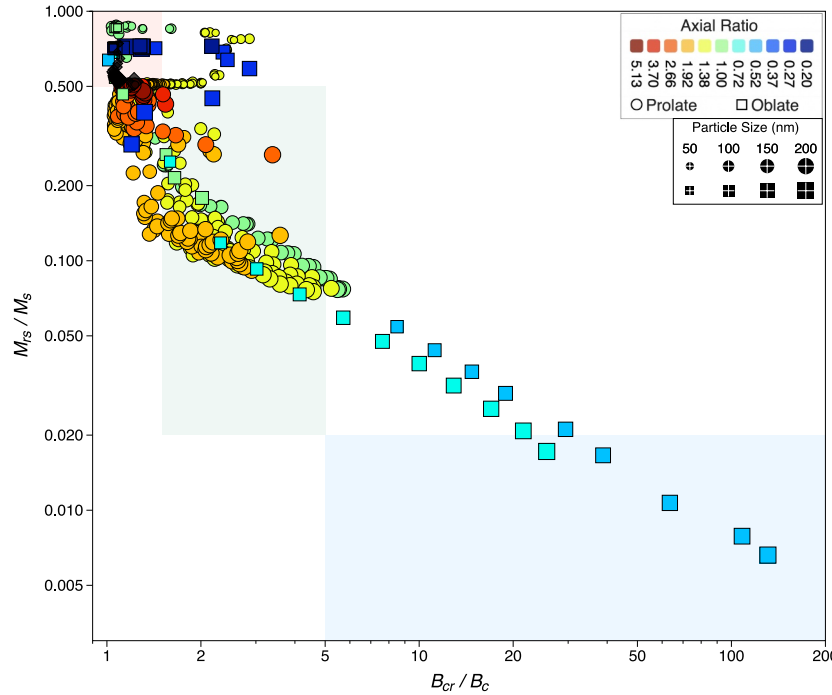


Figure 3. Plot of M_{rs}/M_s versus B_{cr}/B_c for simulated magnetite mono-dispersions with increasing particle size and axial ratio. Oblate and prolate particles are represented by square and round symbols respectively, and colored according to their axial ratio. Symbol sizes are proportional to the particle sizes. Single domain, pseudo-single-domain, and multi-domain regions proposed by Day et al. (1977) are indicated by the lightly shaded red, green and blue regions, respectively.

that are distinctive to SD particles with a set anisotropy symmetry. The first is at $M_{rs}/M_s = 0.87$, which reflects the cubic magnetocrystalline anisotropy expressed in near-equidimensional particles (AR ≈ 1, colored green in Figure 4). The second group is at $M_{rs}/M_s \sim 0.71$, as expected for highly oblate particles (AR $\lessapprox$ 0.5, colored blue) with a four-fold projection of the cubic magnetocrystalline anisotropy into the oblate plane (see Table 1). The third group is for highly prolate particles (AR $\gtrapprox$ 1.3, colored orange to red), where uniaxial shape anisotropy dominates, yielding $M_{rs}/M_s \sim 0.5$. Elongated particles with SD-like domain states show M_{rs}/M_s values up to 2% larger than the expected value of 0.5, due to the faceted morphology of the grains that indicates a small multi-axial configurational anisotropy (Williams et al., 2006).

Similarly, analytical calculations of B_{cr}/B_c for distributions of SD particles with coherent switching (Joffe & Heuberger, 1974) predict that B_{cr}/B_c is also influenced by magnetic anisotropy, but to a lesser degree. For a distribution of particles with the same anisotropy symmetry we expect the following B_{cr}/B_c ratios: 1.08 (uniaxial), 1.15 (platelets) and 1.04/1.09 (positive/negative cubic) (Joffe & Heuberger, 1974). For a distribution of SD particles with mixed anisotropies, Gaunt (1960) obtained $B_{cr}/B_c \lessapprox 2$. While our models are broadly consistent with these analytic predictions, in some cases we can obtain B_{cr}/B_c ratios approaching 3.0 even for particles of the same anisotropy form, but where neither shape nor magnetocrystalline anisotropies dominate, so producing a more complex overall magnetic anisotropy. This occurs in particles with AR values ≈ 1.3 (yellow points) and ≈0.25 (medium blue points) for prolate and oblate particles, respectively.

In addition to prolate and oblate particles, the modeled cruciform structures represent the more complex "skeletal" particle structures observed in many basalts (Tauxe et al., 2002). In these morphologies, all particles up to the maximum modeled size of 200 nm are SD-like, with the magnetization in each limb aligned to the limb axis. As particle size increases, the magnetization at the end of each limb becomes increasingly flowered (e.g., Figures 2j–2l), which causes M_{rs}/M_s to gradually decrease with increasing ESVD particle size from a maximum of 0.74 for the 40 nm particle to 0.52 at 200 nm. The cruciform structures have B_{cr}/B_c values that remain relatively constant between 1.04 and 1.1. Hidden in the B_{cr}/B_c ratio is the fact that the coercivity (B_c) of cruciform particles can be much larger than that expected for SD particles, which was why Tauxe et al. (2002) argued for plotting M_{rs}/M_s versus B_c or B_{cr} separately.

15252027, 2024, 8, Downloaded from https://agupubs.onlinelibrary.wiley.com/doi/10.1029/2024GC011462 by Test, Wiley Online Library on [07/08/2024]. See the Terms and Conditions (https://onlinelibrary.wiley.com/terms-and-conditions) on Wiley Online Library for rules of use; OA articles are governed by the applicable Creative Commons License

15252027, 2024, 8, Downloaded from https://agupubs.onlinelibrary.wiley.com/doi/10.1029/2024GC011462 by Test, Wiley Online Library on [07/08/2024]. See the Terms and Conditions (https://onlinelibrary.wiley.com/terms-and-conditions) on Wiley Online Library for rules of use; OA articles are governed by the applicable Creative Commons License

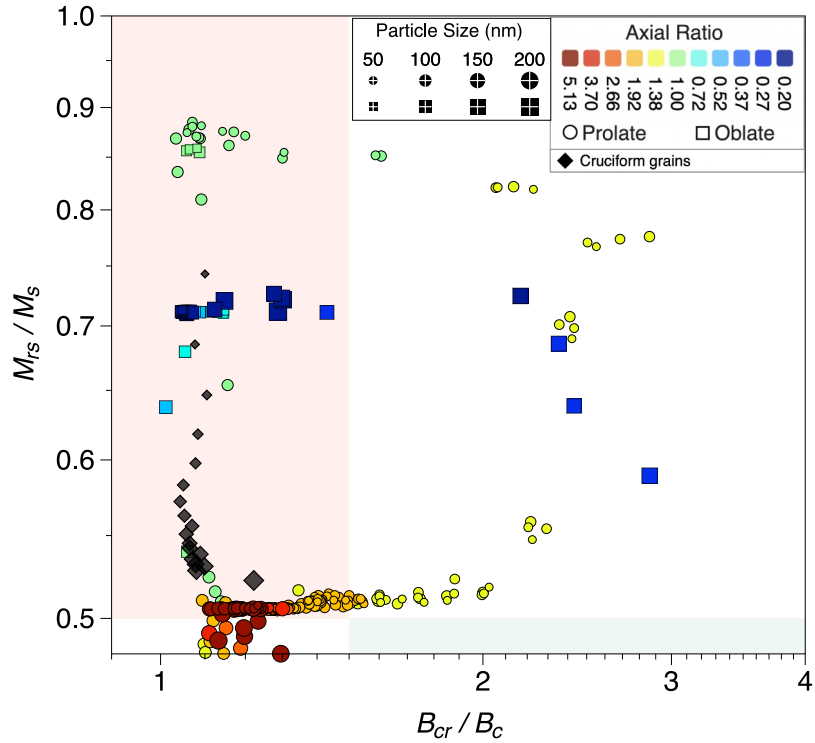


Figure 4. An enlarged section of Figure 3 with results for modeled mono-dispersions of single domain (SD) particles. Symbols are colored according to the particle's axial ratios, with circles and squares used for prolate and oblate particles respectively for additional clarity. The cruciform structures are shown as black diamonds. Symbol sizes are proportional to the particle sizes. The Day plot SD and pseudo-single domain regions are colored as Figure 3.

3.2. SV Particle Behavior on the Day Plot

The Day plot parameters for modeled SV prolate particles fall within the PSD boundaries of $0.02 < M_{rs}/M_s < 0.5$ but slightly outside the $1.5 < B_{cr}/B_c < 4$ limits, as defined by Day et al. (1977). Immediately below the $M_{rs}/M_s = 0.5$ boundary, domain states in any particular particle size are generally a combination of SD and SV, with SV states increasingly dominant as M_{rs} falls further. As the size of prolate particles increases, M_{rs}/M_s decreases, reflecting smaller vortex cores that carry the remanence. Likewise, B_{cr}/B_c also falls, reflecting increasing internal demagnetizing fields as well as the non-coherent domain state switching of the vortex core, referred to as structure coherent rotation (Nagy, Williams, Tauxe, Muxworthy, et al., 2019). For particles of a particular size, increasing elongation or contraction drives a change toward the SD state. SV oblate particles of moderate AR values of ~0.6 have Day-plot parameters that fall well into the MD region. We only consider particles with a maximum ESVD size of 200 nm, well below the expected transition to MV states at ~3 μm (Nagy, Williams, Tauxe, & Muxworthy, 2019), so the trend line for SV particles in Figure 3 might continue into the MD region for all particle morphologies.

Table 1
M_{rs}/M_s for Single Domain Particles for Various Magnetic Anisotropy Symmetries Determined Using Equation 1

Anisotropy type	M_{rs}/M_s	Easy direction	θ limits	ϕ limits
Uniaxial	0.500	[1,0,0]	0, $\pi/2$	0, 2π
Three fold in basal plane	0.649	$\frac{1}{2}[1,\sqrt{3},0]$	0, $\pi/2$	0, $2\pi/3$
Four fold in basal plane	0.707	$\frac{1}{\sqrt{2}}[1,1,0]$	0, $\pi/2$	0, $\pi/2$
Six fold in basal plane	0.750	$\frac{1}{2}[\sqrt{3},1,0]$	0, $\pi/2$	0, $\pi/3$
Easy basal plane	0.785	[cos ϕ, sin ϕ, 0]	0, $\pi/2$	0, 2π
Cubic $K > 0$	0.832	[1,0,0]	0, θ_{mid} [a]	0, 2π
Cubic $K < 0$	0.866	$\frac{1}{\sqrt{3}}[1,1,1]$	0, $\pi/2$	0, 2π

Note. The specified integration limits for the azimuthal angle (ϕ) and polar angle (θ) define the anisotropy symmetry about the given easy direction for each anisotropy type. [a] $\theta_{mid} = \tan^{-1}\left(\frac{1}{\cos\phi}\right)$.

4. Discussion

The Day Plot is an attempt to characterize the domain state/particle size of an assemblage of magnetic particles in a sample using the ratio of four experimentally measured parameters, that is, M_{rs}/M_s and B_{cr}/B_c. While there have been many studies on the merits and shortfalls of using Day plots as indicators of domain state, until recently it has not been possible to account for the presence of pseudo-single-domain (PSD) states. Within the SV particle size range, the vortex structure will distort to accommodate irregular and

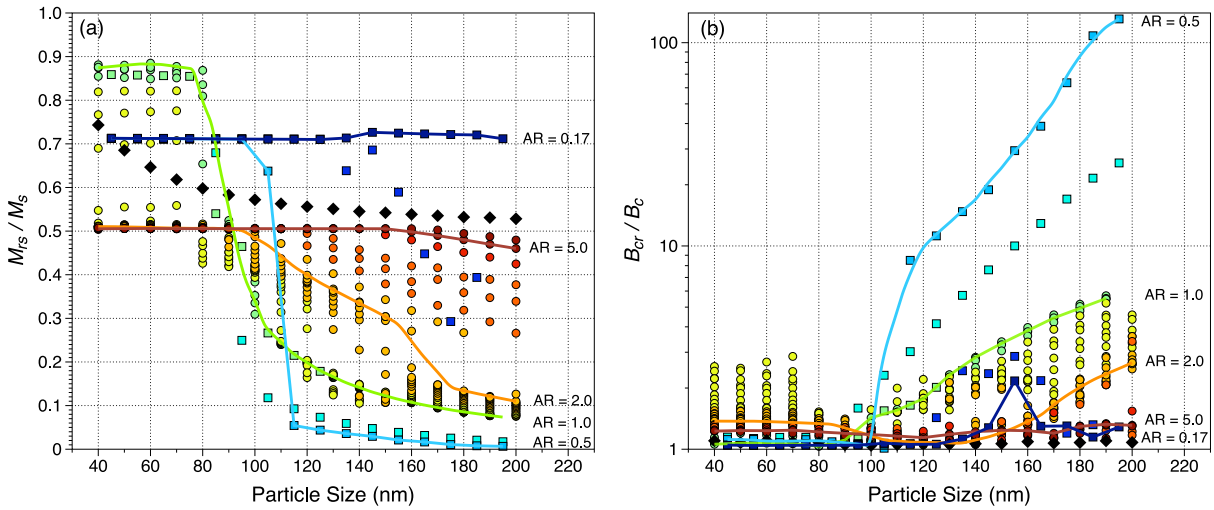


Figure 5. Plot of (a) M_{rs}/M_s and (b) B_{cr}/B_c versus particle size (equivalent spherical volume diameters) for randomly aligned mono-dispersions of truncated-octahedral magnetite with different axial ratios (AR), as well as 3D cruciform geometries. The data points are colored according to particle AR. Lines for particles of selected equal ARs are drawn for clarity.

asymmetric particle morphologies, and so we regard asymmetric SV domain states to be included within this broad category. Numerical micromagnetic models provide an insight into magnetic behavior in idealized stoichiometric mineral structures by relaxing the constraint of uniform magnetization and coherent domain state switching that have limited much of our present understanding of magnetic recordings in paleomagnetic samples.

4.1. The Day Plot and Particle Size Discrimination for Monodisperse Magnetite

Of the two ratios, variation of M_{rs}/M_s with the domain state dependent particle size is the easiest to predict and understand. For a population of SD particles, in the absence of significant SP particle content, extensive "flowering" or inter-particle magnetic interactions, M_{rs}/M_s does not fall below 0.5. In contrast, our models predict that no SV states are possible with $M_{rs}/M_s > 0.5$ (Figure 5a), however, this ratio by itself is not a direct indicator of particle size due to non-uniqueness in M_{rs}/M_s. Since B_c and B_{cr} reflect both reversible and irreversible domain state changes as a function of applied field, it is anticipated that non-coherent switching mechanisms that dominate in larger particles will also affect B_{cr}/B_c. Dunlop and Özdemir (1997) noted that non-coherent switching will result in lower critical fields and thus lower B_{cr} and B_{cr}/B_c ratios. We might expect B_{cr}/B_c to decrease for SD particles as they near the critical particle size where SD switching can occur via a transitory vortex state (Enkin & Williams, 1994). While this effect is imperceptible in most mono-dispersions of a single anisotropy, a B_{cr} decrease is noticeable in Figure 6 for particles with AR = 1.0 and AR = 1.25 as the particles grow toward the critical particle size of ≈80 and ≈90 nm, respectively (Butler & Banerjee, 1975; Moreno et al., 2022; Muxworthy & Williams, 2006).

4.2. The Effect of Particle Shape

The trend line for SV domain states on a log-log Day plot (Figure 3) is remarkably linear within the 40–200 nm particle size range modeled. The lack of data scatter is partly due to the single truncated-octahedral particle shape, which has been elongated or compressed to form prolate or oblate morphologies. All prolate and oblate particles below 195 nm nucleate domain states that are either in the SD or SV state. In Figure 7, we compare our data against the simulated Day plot parameters in particles with irregular morphologies from Nikolaisen et al. (2020). Since almost all of their irregular particles have a triaxial morphology, matching can only be approximate. Nevertheless, there is good agreement between the Day plot trend from the irregular data and that from our idealized prolate and oblate particles.

It is worth noting that several irregular geometries (marked with hexagons in Figure 7) are stated to have MV domain states (see Figure 5 of Nikolaisen et al. (2020)), yet their Day plot parameters place them near the SD-SV boundary. These data points contradict our results, which indicate that no MV state should yield M_{rs}/M_s values

15252027, 2024, 8, Downloaded from https://agupubs.onlinelibrary.wiley.com/doi/10.1029/2024GC011462 by Test, Wiley Online Library on [07/08/2024]. See the Terms and Conditions (https://onlinelibrary.wiley.com/terms-and-conditions) on Wiley Online Library for rules of use; OA articles are governed by the applicable Creative Commons License

15252027, 2024, 8, Downloaded from https://agupubs.onlinelibrary.wiley.com/doi/10.1029/2024GC011462 by Test, Wiley Online Library on [07/08/2024]. See the Terms and Conditions (https://onlinelibrary.wiley.com/terms-and-conditions) on Wiley Online Library for rules of use; OA articles are governed by the applicable Creative Commons License

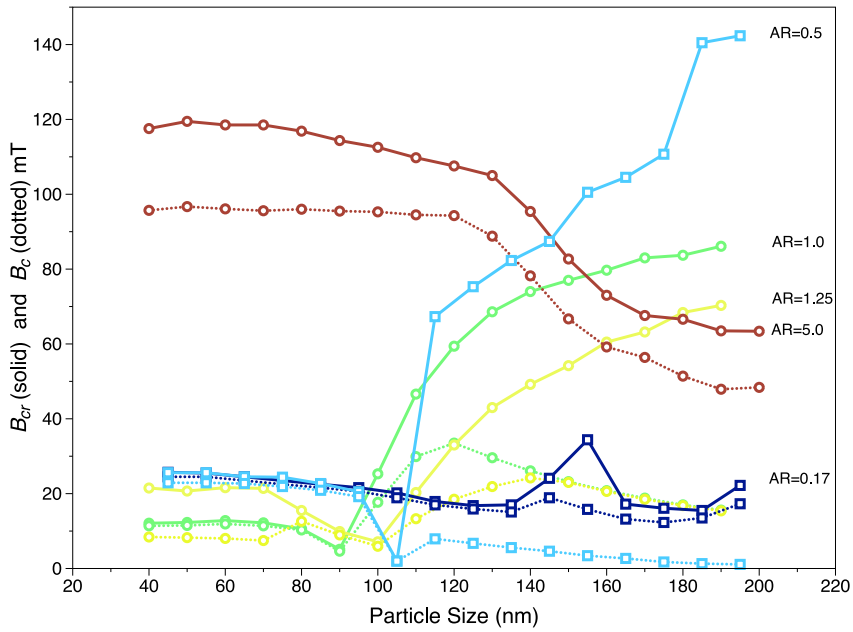


Figure 6. Plot of B_{cr} (solid lines) and B_c (dotted lines) versus particles size for randomly aligned mono-dispersions of truncated-octahedral magnetite of different selected axial ratios.

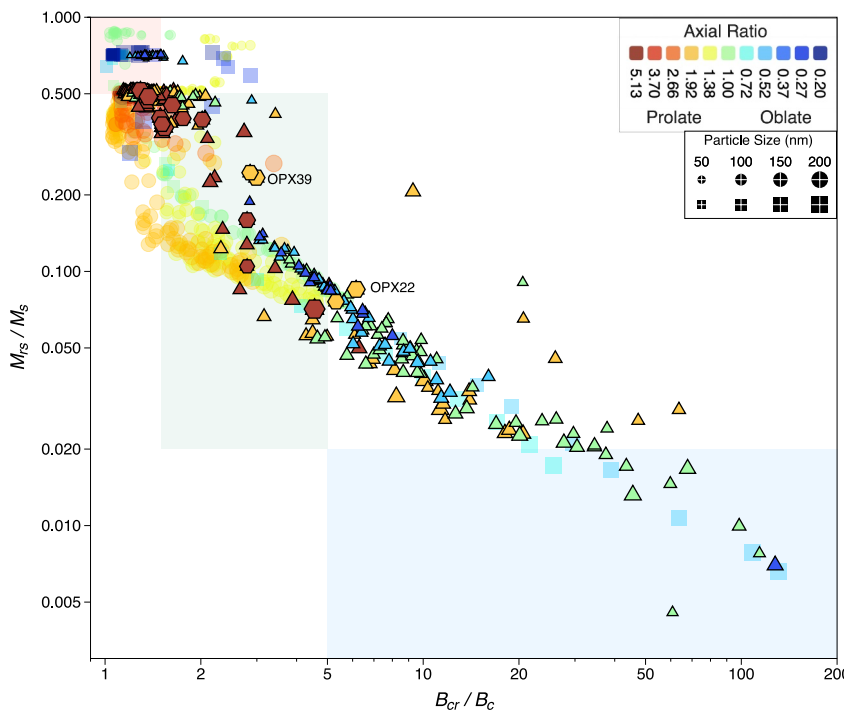


Figure 7. Day Plot for irregular particle morphologies from Nikolaisen et al. (2020). Colored triangles and hexagons are superimposed on the data for prolate and oblate truncated-octahedral particles from this study (made translucent for clarity). Data from Nikolaisen et al. (2020) are colored according to their parameter ob-pro-sph = log((a − b)/(b − c)), where a, b, c are the particle long, intermediate and short axis lengths, scaled to match the axial ratio range of this study. Triangle symbols indicate single domain or single-vortex domain states, while hexagons indicate multi-vortex states. Symbol sizes are scaled to particle size in the same way for both data sets.

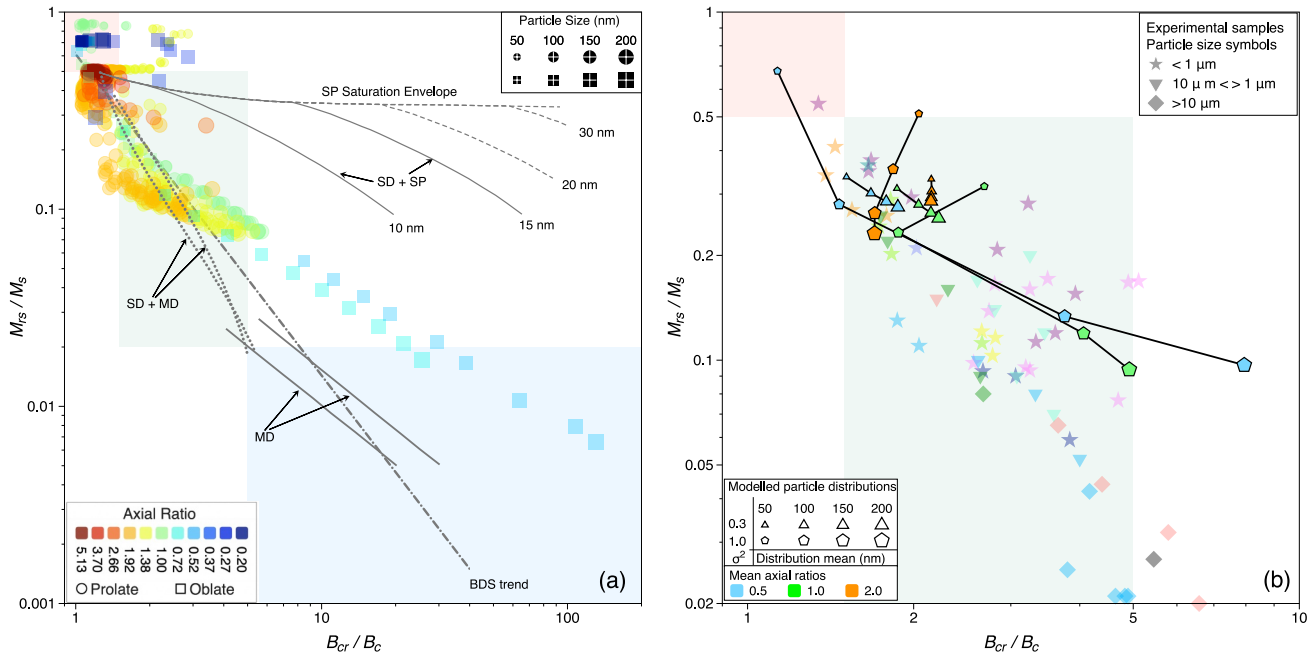


Figure 8. (a) Day Plot for our numerical models (translucent dots and squares) compared to analytic model predictions of domain state mixtures (gray lines), and (b) log-normal particle size and shape distributions from our numerical solutions (black lines and colored diamonds). Lines for single domain (SD) + multidomain (MD), SD + superparamagnetic and MD are from Dunlop (2002a), and the bulk domain stability trend line is from Paterson et al. (2017). Modeled particle distributions in (b) are described in the text. Particle size and axial ratio legends apply to the model data for mono-dispersions in (a) and to the geometric means of the modeled log-normal distributions in (b). Translucent colored stars, inverted triangles and diamonds are colored according to the data attribution in Figure 9. An alternate form of these plots are provided in Supporting Information S1 (Figure S3), to aid comparison of modeled distributions to both the synthetic and experimental data.

greater than 0.5, so we further investigated these specific morphologies from Nikolaisen et al. (2020) by re-running their local energy minimum. For each published irregular geometry, we calculated 100 models starting from different random initial states. Our results show that these irregular particle structures support a variety of domain states (see Figure S2 in Supporting Information S1), with particles as small as 163 nm sometimes being able to host MV domain states. A greater variety of domain states in these cases also reflects a variety of final energies for each of the 100 solutions. In many of these geometries, MV states are often one of the less frequent higher energy states. In such particles, simulated hysteresis and backfield measurements will inevitably average over several domain states nucleated as a result of varying the applied field direction. Consequently, these are likely to be dominated by the lower energy domain states, often SV, and the saturated remanence states during hysteresis. Two particles highlighted in Figure 7, OPX39 and OPX22, both have MV structures as their lowest energy states, but even these particles yield M_{rs}/M_s values well above those expected for MD states and are likely to hold stable magnetic remanences (Shah et al., 2018). The overall good agreement between the idealized particle morphologies and the irregular particles suggests that, as in the case of SD particles, much of the general behavior of SV/PSD particles can be determined by examining simple particle geometries.

4.3. Comparison to Analytic Models (Mixing Models)

So far we have considered Day plot parameters for magnetite mono-dispersions with idealized morphologies, but experimental observations (except for samples created by etching of thin films; King et al., 1996; Krása et al., 2009) will inevitably be representative of a variety of particle sizes and domain states. Dunlop (2002a) explored the Day plot in terms of mixtures of SD and MD particles, and concluded that such mixtures can plot in the PSD region for a wide range of SD/MD mixtures (see his mixing models in Figure 8a). Dunlop (2002a) demonstrated that while SP particles can significantly increase B_{cr}/B_c, M_{rs}/M_s never decreases below ≈0.09, even for samples containing a >80% SP fraction; such mixtures should be easily distinguished from samples dominated by MD particles. Mixtures of ideal SD and MD particles produce trend lines that fall within the expected PSD Day plot region, and demonstrate that samples containing such mixtures cannot be distinguished from samples dominated by PSD particles. The SD + MD mixture trend lines were formulated to explain Day plot behavior in

15252027, 2024, 8, Downloaded from https://agupubs.onlinelibrary.wiley.com/doi/10.1029/2024GC011462 by Test, Wiley Online Library on [07/08/2024]. See the Terms and Conditions (https://onlinelibrary.wiley.com/terms-and-conditions) on Wiley Online Library for rules of use; OA articles are governed by the applicable Creative Commons License

15252027, 2024, 8, Downloaded from https://agupubs.onlinelibrary.wiley.com/doi/10.1029/2024GC011462 by Test, Wiley Online Library on [07/08/2024]. See the Terms and Conditions (https://onlinelibrary.wiley.com/terms-and-conditions) on Wiley Online Library for rules of use; OA articles are governed by the applicable Creative Commons License

the absence of any detailed understanding of the hysteresis in PSD particles. Calculations presented here, together with the work of Nikolaisen et al. (2020), demonstrate that mono-dispersions of SV particles fall within the expected Day plot region for PSD particles without the need to consider mixtures of other domain states. It is important to note, however, that both the work of Dunlop (2002a, 2002b) and Nikolaisen et al. (2020) as well as the work presented here show that the PSD region is not necessarily constrained to the domain state boxes as defined by Day et al. (1977) or Dunlop (2002a). Any boundary should be regarded as "soft" and the square boxes regarded only as a very approximate guide.

Within the particle size range of our numerical solutions, we can construct more realistic size distributions by linearly averaging hysteresis and remanence backfield curves with suitable weightings. In Figure 8b we show Day plot parameters for 24 lognormal distributions plotted together with experimental observations on sized mono-dispersions. Day plot parameters for the lognormal distributions can be generated from our Synth-FORC application at https://synth-forc.earthref.org (Nagy, Moreno, Williams, et al., 2024). Each modeled distribution is characterized by the geometric mean $\bar{d}$ and $\overline{AR}$ of the particle size and axial ratio respectively. The lognormal distributions are similar to those produced in the laboratory, for example, samples of Argyle and Dunlop (1990) and Ge et al. (2021). The 24 distributions we model can be categorized into two groups based on the distribution widths, which are ($\sigma^2 = 0.3$ (narrow) or $\sigma^2 = 1.0$ (wide)) chosen to bound the experimentally observed distribution widths. The same value of σ^2 is used for both the grain size and axial ratio. For the narrow and wide distributions, we consider three different mean AR, $\overline{AR}$, of 0.5 (blue symbols), 1.0 (green symbols) and 2.0 (orange symbols) with distributions of equal $\overline{AR}$ joined by a black line. We then have four different mean particle sizes $\bar{d}$, of 50, 100, 150, and 200 nm, where the symbol size used is proportional to $\bar{d}$. The effect of hysteresis data and back-field curve averaging is to move their Day plot parameters to the centroid of the bounding Day plot region containing the particles in the distribution. These averages suggest that the narrow range of axial ratios (AR $\approx$ 0.5) for oblate particles responsible for the high B_{cr}/B_c ratio seen in Figure 3 is quickly reduced and so is not noticeable even in experimental mono-dispersions. It is important to point out that the maximum grain size in our modeled distributions is 200 nm, any log-normal distributions whose tail extends beyond this are nevertheless truncated at 200 nm. Inclusion of multi-vortex and multidomain states is currently beyond what we are able to model in sufficient detail, but are clearly needed to improve the fit to experimental data.

4.4. Comparison With Experimental Samples

In the original Day plot (Day et al., 1977) divisions of SD to PSD and PSD to MD were made based on experimental observations in titanomagnetites together with theoretical limits of SD structures (Butler & Banerjee, 1975; Stoner & Wohlfarth, 1948). Since the Day plot was published, there have been attempts to validate the theoretical predictions by observations on well-characterized particle sized-dispersions of magnetites (Argyle & Dunlop, 1990; Bailey & Dunlop, 1983; Dankers & Sugiura, 1981; Day et al., 1977; Dunlop, 1986; Heider et al., 1996; Krása et al., 2011; Muxworthy, 1998; Muxworthy & McClelland, 2000; Muxworthy et al., 2006; Özdemir & Banerjee, 1982); many of these are shown in Figure 9. Except for the elongated particles of Dunlop (1986), the experimental data are from near equidimensional particles, similar to the geometries used in our models. While there is generally good agreement, the experimental data do not have the high B_{cr}/B_c values predicted for oblate particles of our study nor the highly irregular triaxial particle geometries of Nikolaisen et al. (2020). This is likely due to averaging effects seen in broader particle size distributions.

For equidimensional particles, there is a noticeable difference in the gradient of the ratio of $(M_{rs}/M_s)/(B_{cr}/B_c)$ in the PSD region, with this being larger for experimental mono-dispersions than in the numerical models. However, production of laboratory-manufactured samples that are true analogs of natural rocks is difficult. In addition to the sized natural samples (labeled "N" in the legend of Figure 9), there are three main types of laboratory samples: (a) those that are sized by crushing larger particles; (b) those that are grown and remain un-crushed; (c) and those that are produced by etching epitaxial films to produce specific particle sizes and inter-particle separations, noted by the letters "C," "G," and "E" (Figure 9). Each method has its advantages and disadvantages, with only the etched samples guaranteed to be free from inter-particle magnetostatic interactions. Data for these few samples appear to be in better agreement with the numerical models. Nevertheless, they are also likely to be significantly stressed due to the mismatch between the unit cell size of magnetite and that of the ruby substrate upon which they were grown (King et al., 1996; Krása et al., 2011). Powdered samples suffer from the effects of magnetostatic interactions, which decrease M_{rs}/M_s (and to a lesser extent B_{cr}/B_c (Muxworthy et al., 2003)). The latter will

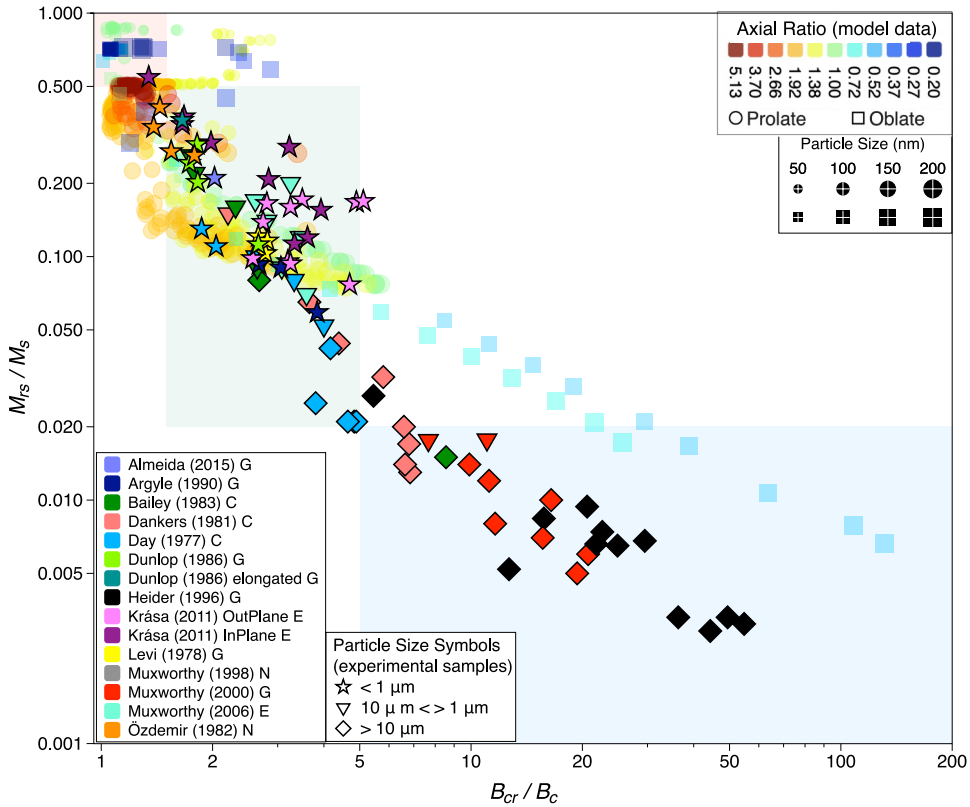


Figure 9. Plot of our modeled Day Plot parameters, (translucent) colored by their axial ratio, against those of sized experimental samples in black outlined symbols, colored to identify the original study from which the data were obtained. Experimental samples are also categorized by their laboratory particle processing as, grown (G), crushed (C), etched thin films (E), or natural crystals (N). Thin film samples are further categorized by whether the field was applied in- or out-of-plane of the film. Different symbol shapes, shown in the legend, to identify the vortex to multidomain boundary, the lower limit of which is ~1 μm and the upper limit ~10 μm.

consequently bias the experimental data toward steeper gradients on the Day Plot. Within these limitations, there is good agreement between the properties of laboratory-produced particles and our numerical simulations.

4.5. Alternatives to the Day Plot

The benefit of plotting M_{rs} normalized by M_s, and B_{cr} normalized by B_c is that for SD particles these ratios should be independent of mineralogy, except where that is expressed in their different magnetic anisotropies; the SD Day plot region should be distinct across different experimental samples. This is not necessarily true for MD particle distributions, as clearly shown for hematite by Özdemir and Dunlop (2014). The low intrinsic magnetization of hematite results in weak internal demagnetizing fields, H_d, such that domain wall motion is determined almost entirely by the externally applied field. Thus, values of $B_c \approx B_{cr}$ and near saturation values of M_{rs}/M_s often over 0.9 (Özdemir & Dunlop, 2014) are observed, which is far greater than the M_{rs}/M_s SD limit of 0.75 for hematite.

Alternatives to the Day plot such as diagrams of M_{rs}/M_s against either B_c or against B_{cr}, first used by Néel (1955) and shown in Figure 10, have also been explored to discriminate between magnetic domain states (e.g., Roberts et al., 2019; Tauxe et al., 2002). Generally, we expect coercivities to decrease with increasing particle size, as the domain switching mechanism changes from coherent rotation to non-coherent mechanisms, specifically vortex core rotation, and vortex core nucleation, translation and denucleation (Enkin & Williams, 1994). All non-coherent domain state changes are indications that significant internal demagnetizing fields exist within a particle, but the absolute values will vary with mineralogy. With a single dominant mineralogy, the coercivities can sometimes also indicate particle morphology. For example, equidimensional magnetite particles have magnetocrystalline anisotropy-controlled coercivities no greater than ~37 mT (Williams & Dunlop, 1995); values larger

15252027, 2024, 8, Downloaded from https://agupubs.onlinelibrary.wiley.com/doi/10.1029/2024GC011462 by Test, Wiley Online Library on [07/08/2024]. See the Terms and Conditions (https://onlinelibrary.wiley.com/terms-and-conditions) on Wiley Online Library for rules of use; OA articles are governed by the applicable Creative Commons License

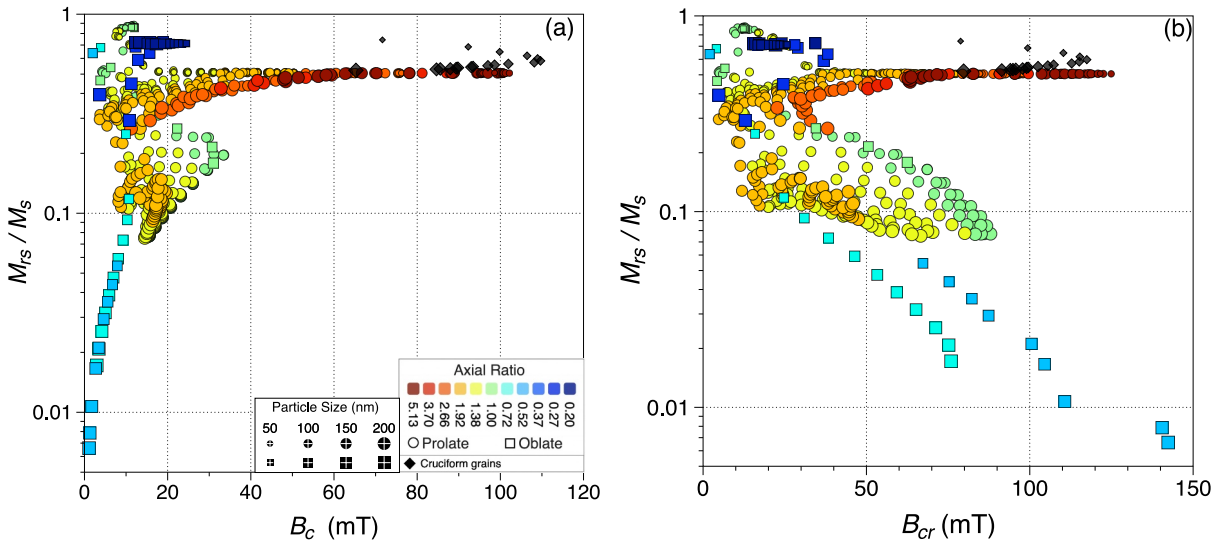


Figure 10. Plots of (a) M_{rs}/M_s versus B_c, often referred to as a Néel plot, and (b) M_{rs}/M_s versus B_{cr}. The legend for axial ratio and particle size apply to both plots.

than this will indicate the presence of particles dominated by shape or configurational anisotropy. This is seen in Figure 10 for prolate particles of similar M_{rs}/M_s whose B_c and B_{cr} increases with AR (Tauxe et al., 2002). However this is not true in general, and neither oblate nor the more complex cruciform-shaped particles (or the triaxial particles reported by Nikolaisen et al. (2020)) exhibit such a clear variation with AR.

Plotting M_{rs}/M_s against B_{cr} (Figure 10b) does not yield a monotonic decrease in the abscissa observed in the Day plot. However, both M_{rs} and B_{cr} measure the remanence domain states that are important to paleomagnetic studies, rather than the induced domain states of in-field measurements. B_{cr} observations thus avoid the contamination of superparamagnetic (SP) and weakly stable (MD) states that lower both the value of M_{rs}/M_s and B_{cr}/B_c (Dunlop, 2002a). This avoids the issue in the Day plot where samples containing mixtures of SP together with stable SD and SV particles are place in the MD region of the Day plot, falsely indicating the sample to be a poor paleomagnetic recorder. We might also expect B_{cr} to be an indicator of changing domain state because B_{cr} increases with the internal demagnetizing field, which acts to restore the domain state on removal of the external field. Increasing internal demagnetizing fields are also precursors to domain state changes, which form to minimize the internal field. We therefore expect to see a decrease in B_{cr} at the critical SD particle size d_c on the transition to SV states, and also at the critical vortex domain size d_v on the transition to MD states.

Near the SD-PSD boundary our models indicate there is a slight decrease in B_{cr} due to vortex state nucleation (Figure 5), but this is a subtle effect and is likely not resolvable in anything other than mono-dispersions. We might expect a larger change in B_{cr} near the transition to MD states at d_v. At present we can not model such large particles but experimental observations for sized particle distributions (Figure 11), does show a marked decrease in B_{cr} at ~1–10 μm, at the predicted d_v size in magnetite (Nagy, Williams, Tauxe, & Muxworthy, 2019). Thus, in the Day plot alternative of M_{rs}/M_s against B_{cr}, the upper left hand side of the plot should contain SD particles. M_{rs}/M_s will decrease monotonically with particle size, but B_{cr} should rise and fall at each major domain state transition. This is apparent experimentally in sized particle samples but likely difficult to distinguish in natural samples. Critically, absolute B_{cr} values will depend on mineralogy, so interpretation would depend on samples with a single dominant mineralogy, and availability of B_{cr} reference values for SD, PSD, and MD particles. For example, the easy basal plane anisotropy and weak magnetization of hematite results in MD particles with high M_{rs}/M_s values and low B_{cr}/B_c values, so they lie well into SD Day plot region (for a single dominant mineral, MD hematite is best identified by $M_{rs} \sim 0.75$) (Özdemir & Dunlop, 2014). In this case, the Néel plot would yield high coercivities that might be diagnostic of a mineral such as hematite. Alternatively, since we expect B_{cr} to increase the internal demagnetizing field H_d value, we might expect B_{cr} to peak before a domain state change and so plotting M_{rs}/M_s against B_{cr} would not only produce a high B_{cr} value that provides a guide to mineralogy, but its value should peak before a domain state change. A B_{cr} peak occurs near 1 μm for magnetite in Figure 11, in broad agreement with the theoretically predicted value of ~3 μm (Nagy, Williams, Tauxe, & Muxworthy, 2019), and the

15252027, 2024, 8, Downloaded from https://agupubs.onlinelibrary.wiley.com/doi/10.1029/2024GC011462 by Test, Wiley Online Library on [07/08/2024]. See the Terms and Conditions (https://onlinelibrary.wiley.com/terms-and-conditions) on Wiley Online Library for rules of use; OA articles are governed by the applicable Creative Commons License

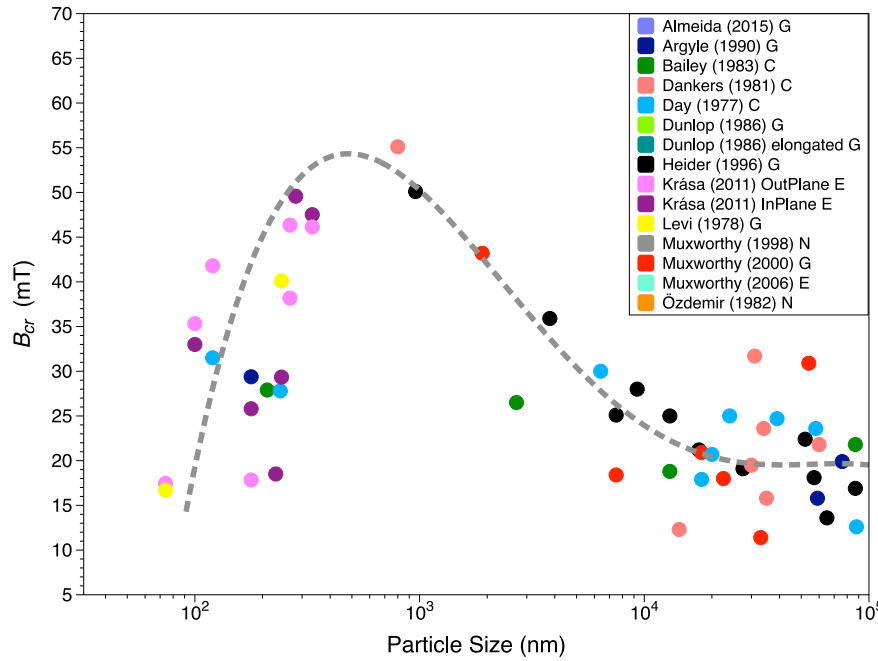


Figure 11. B_{cr} variation with particle size, from experimental observations on sized particle distributions. The symbols are colored according to data attribution as shown in the legend (as in Figure 9). The dashed gray line is drawn as a guide to the eye.

experimentally determined value of ~0.8 μm (Dunlop & Özdemir, 1997, p. 153). However, the variation in B_{cr} with particle size is likely too weak to be useful in any predictive test on paleomagnetic samples.

5. Conclusions

Characterization of the magnetic properties of a natural sample using a single data point can only ever be expected to provide a bulk estimate of its domain state, particle size or paleomagnetic stability. Each mono-dispersion that we model may contain a variety of domain states if more than one state is supported in particles of that size and shape. Usually, mono-dispersions will be dominated by one domain state type (SV or SD) except for particles near the critical SD particle size d_c. In our magnetite particles with idealized shape and stoichiometry (ranging from 40 to 200 nm), we observe a Day plot trend similar to those predicted for irregular particle shapes (Nikolaisen et al., 2020). This suggests that despite the simple geometries we impose, they can make broad predictions of the hysteresis characteristics of particles in natural samples. Our predictions of Day plot parameters are consistent with experimental observations on laboratory-manufactured samples, particularly when averaged over log-normal distributions typical of laboratory-made samples.

For SD particles, our results indicate that while we obtain the expected M_{rs}/M_s values above 0.5, we can have B_{cr}/B_c values as large as 3 for particles where neither shape nor magnetocrystalline anisotropy dominate (see Figure 4; the data plot well outside the traditional B_{cr}/B_c SD limit of 1.5; Day et al. (1977)). Mono-dispersions of SV domain states have M_{rs}/M_s values below 0.5 that decrease with increasing particle size. For a narrow range of oblate morphologies with both shape and magnetocrystalline anisotropy (AR ≈ 0.2), we obtain M_{rs}/M_s much smaller than the lower PSD limit of 0.02, and B_{cr}/B_c far larger than 4 (Day et al., 1977) or 5 (Dunlop, 2002a) and so are more indicative of MD domain states. In our models of log-normal distributions of SD and SV domain states, the contribution of the relatively narrow band of SV particles with large B_{cr}/B_c values is not noticeable. For natural samples, however, Nikolaisen et al. (2020) reported a larger abundance of SV particles with large B_{cr}/B_c values. We cannot therefore exclude the possibility that SV domain states will plot within the MD region of the Day plot.

In bulk samples, there is a likelihood of a range of particle sizes and shapes, as well as a mixture of mineralogies. Often we are interested to know whether this mixture of mineral particles is capable of holding a reliable paleomagnetic signal. The theoretical confirmation that SV and MV particles are at least as magnetically stable as

15252027, 2024, 8, Downloaded from https://agupubs.onlinelibrary.wiley.com/doi/10.1029/2024GC011462 by Test, Wiley Online Library on [07/08/2024]. See the Terms and Conditions (https://onlinelibrary.wiley.com/terms-and-conditions) on Wiley Online Library for rules of use; OA articles are governed by the applicable Creative Commons License

SD states (Nagy et al., 2017; Nagy, Williams, Tauxe, Muxworthy, et al., 2019; Shah et al., 2018) suggests that the most important discrimination should be between PSD and MD particles rather than SD and PSD. If that is accepted, then samples with hysteresis parameters within the broad SD and PSD Day plot region are likely to contain a significant proportion of paleomagnetically stable domain states.

Domain state boundaries cannot be regarded as anything other than an approximate guide. This is because domain states themselves are often a continuum, from SD to flower, or S states, to twisted flower to vortex, distorted and multi vortex and multidomain states. The Day plot is an attempt to characterize a sample into just one domain state, and even for a single dominant mineral it is at best an average. Mixtures of minerals add further complications. Absolute B_c and B_{cr} values can help identify Day plot "outliers" but no one diagnostic test should be used in isolation.

Data Availability Statement

All results reported here were generated using MERRILL, the open source micromagnetic modeling code of Ó Conbhuí et al. (2018). Executable LINUX, MacOS and Windows versions of MERRILL used for this study are available in Williams, Paterson, and Nagy (2024). Source code for MERRILL is available from Williams, Fabian, et al. (2024) and is provided under a CC-BY-SA 4.0 International license.

Acknowledgments
We thank David Dunlop, Andrew Roberts and an anonymous reviewer for helpful reviews that significantly enhanced the paper. W.W. and A.R.M. acknowledges support from Natural Environmental Research Council (NERC) Grants NE/S001018/1 and NE/V001388/1. L.N. acknowledges funding from NERC Independent Research Fellowship NE/V014722/1. L.T., W.W. and L.N. acknowledge support of NSFGEO-NERC Grant EAR1827263. G.A.P. acknowledges funding from NERC Independent Research Fellowship (NE/P017266/1) and Grant NE/W006707/1. L.T., G.A.P, and L. N. acknowledge NSFGEO-NERC Grants EAR1827263 and NE/Y005686/1.

References

Almeida, T. P., Kasama, T., Muxworthy, A. R., Williams, W., Nagy, L., Hansen, T. W., et al. (2014). Visualized effect of oxidation on magnetic recording fidelity in pseudo-single-domain magnetite particles. *Nature Communications*, *5*(1), 5154. https://doi.org/10.1038/ncomms6154

Argyle, K. S., & Dunlop, D. J. (1990). Low-temperature and high-temperature hysteresis of small multidomain magnetites (215–540 nm). *Journal of Geophysical Research*, *95*(B5), 7069–7083. https://doi.org/10.1029/jb095ib05p07069

Bailey, M. E., & Dunlop, D. J. (1983). Alternating field characteristics of pseudo-single domain (2–14 μm) and multidomain magnetite. *Earth and Planetary Science Letters*, *63*(3), 335–352. https://doi.org/10.1016/0012-821x(83)90108-5

Brown, W. (1963). Thermal fluctuations of a single-domain particle. *Physical Review*, *130*(5), 1677–1686. https://doi.org/10.1103/physrev.130.1677

Butler, R. F., & Banerjee, S. K. (1975). Theoretical single-domain grain size range in magnetite and titanomagnetite. *Journal of Geophysical Research*, *80*(29), 4049–4058. https://doi.org/10.1029/jb080i029p04049

Coreform LLC. (2017). Coreform Cubit, v16.4 (64-bit). Retrieved from https://coreform.com

Dankers, P., & Sugiura, N. (1981). The effects of annealing and concentration on the hysteresis properties of magnetite around the PSD-MD transition. *Earth and Planetary Science Letters*, *56*, 422–428. https://doi.org/10.1016/0012-821x(81)90145-x

Day, R., Fuller, M., & Schmidt, V. A. (1977). Hysteresis properties of titanomagnetites: Grain-size and compositional dependence. *Physics of the Earth and Planetary Interiors*, *13*(4), 260–267. https://doi.org/10.1016/0031-9201(77)90108-x

Dunlop, D. J. (1986). Hysteresis properties of magnetite and their dependence on particle size: A test of pseudo-single-domain remanence models. *Journal of Geophysical Research*, *91*(B9), 9569–9584. https://doi.org/10.1029/jb091ib09p09569

Dunlop, D. J. (2002a). Theory and application of the Day plot (Mrs/Ms versus Hcr/Hc) 1. Theoretical curves and tests using titanomagnetite data. *Journal of Geophysical Research*, *107*(B3), 2056. https://doi.org/10.1029/2001jb000486

Dunlop, D. J. (2002b). Theory and application of the Day plot (Mrs/Ms versus Hcr/Hc) 2. Application to data for rocks, sediments, and soils. *Journal of Geophysical Research*, *107*(B3), 2046. https://doi.org/10.1029/2001jb000487

Dunlop, D. J., & Carter-Stiglitz, B. (2006). Day plots of mixtures of superparamagnetic, single-domain, pseudosingle-domain, and multidomain magnetites. *Journal of Geophysical Research*, *111*(B12), B12S09. https://doi.org/10.1029/2006jb004499

Dunlop, D. J., & Özdemir, O. (1997). *Rock magnetism: Fundamentals and frontiers*. Cambridge University Press. https://doi.org/10.1017/cbo9780511612794.001

Enkin, R. J., & Williams, W. (1994). 3-dimensional micromagnetic analysis of stability in fine magnetic grains. *Journal of Geophysical Research*, *99*(B1), 611–618. https://doi.org/10.1029/93jb02637

Fletcher, E. J., & O'Reilly, W. (1974). Contribution of Fe^{2+} ions to the magnetocrystalline anisotropy constant K1 of $Fe_{3-x}Ti_xO_4$ ($0 < x < 0.1$). *Journal of Physics C: Solid State Physics*, *7*(1), 171–178. https://doi.org/10.1088/0022-3719/7/1/024

Gaunt, P. (1960). A magnetic study of precipitation in a gold-cobalt alloy. *Philosophical Magazine*, *5*(59), 1127–1145. https://doi.org/10.1080/14786436008238321

Ge, K., Williams, W., Nagy, L., & Tauxe, L. (2021). Models of maghematization: Observational evidence in support of a magnetic unstable zone. *Geochemistry, Geophysics, Geosystems*, *22*(3), e2020GC009504. https://doi.org/10.1029/2020gc009504

Hannay, J. H., & Nye, J. F. (2004). Fibonacci numerical integration on a sphere. *Journal of Physics A: Mathematical and General*, *37*(48), 11591–11601. https://doi.org/10.1088/0305-4470/37/48/005

Harrison, R. J., Dunin-Borkowski, R. E., & Putnis, A. (2002). Direct imaging of nanoscale magnetic interactions in minerals. *Proceedings of the National Academy of Sciences of the United States of America*, *99*(26), 16556–16561. https://doi.org/10.1073/pnas.262514499

Heider, F., & Williams, W. (1988). Note on temperature-dependence of exchange constant in magnetite. *Geophysical Research Letters*, *15*(2), 184–187. https://doi.org/10.1029/GL015i002p00184

Heider, F., Zitzelsberger, A., & Fabian, F. (1996). Magnetic susceptibility and remanent coercive force in grown magnetite crystals from 0.1 μm to 6 mm. *Physics of the Earth and Planetary Interiors*, *93*(3–4), 239–256. https://doi.org/10.1016/0031-9201(95)03071-9

Joffe, I., & Heuberger, R. (1974). Hysteresis properties of distributions of cubic single-domain ferromagnetic particles. *Philosophical Magazine*, *29*(5), 1051–1059. https://doi.org/10.1080/14786437408226590

King, J. G., & Williams, W. (2000). Low-temperature magnetic properties of magnetite. *Journal of Geophysical Research*, *105*(B7), 16427–16436. https://doi.org/10.1029/2000jb900006

15252027, 2024, 8, Downloaded from https://agupubs.onlinelibrary.wiley.com/doi/10.1029/2024GC011462 by Test, Wiley Online Library on [07/08/2024]. See the Terms and Conditions (https://onlinelibrary.wiley.com/terms-and-conditions) on Wiley Online Library for rules of use; OA articles are governed by the applicable Creative Commons License

King, J. G., Williams, W., Wilkinson, C. D. W., McVitie, S., & Chapman, J. N. (1996). Magnetic properties of magnetite arrays produced by the method of electron beam lithography. *Geophysical Research Letters*, *23*(20), 2847–2850. https://doi.org/10.1029/96gl01371

Krása, D., Muxworthy, A. R., & Williams, W. (2011). Room- and low-temperature magnetic properties of 2-D magnetite particle arrays. *Geophysical Journal International*, *185*(1), 167–180. https://doi.org/10.1111/j.1365-246X.2011.04956.x

Krása, D., Wilkinson, C. D. W., Gadegaard, N., Kong, X., Zhou, H., Roberts, A. P., et al. (2009). Nanofabrication of two-dimensional arrays of magnetite particles for fundamental rock magnetic studies. *Journal of Geophysical Research*, *114*(B2), B02104. https://doi.org/10.1029/2008jb006017

Lascu, I., Einsle, J. F., Ball, M. R., & Harrison, R. J. (2018). The vortex state in geologic materials: A micromagnetic perspective. *Journal of Geophysical Research-Solid Earth*, *123*(9), 7285–7304. https://doi.org/10.1029/2018jb015909

Moreno, R., Carvalho-Santos, V., Altbir, D., & Chubykalo-Fesenko, O. (2022). Detailed examination of domain wall types, their widths and critical diameters in cylindrical magnetic nanowires. *Journal of Magnetism and Magnetic Materials*, *542*, 168495. https://doi.org/10.1016/j.jmmm.2021.168495

Muxworthy, A. R. (1998). *Stability of magnetic remanence in multidomain magnetite (unpublished doctoral dissertation)*. Univeristy of Oxford.

Muxworthy, A. R., King, J. G., & Odling, N. (2006). Magnetic hysteresis properties of interacting and noninteracting micron-sized magnetite produced by electron beam lithography. *Geochemistry, Geophysics, Geosystems*, *7*(7), Q09003. https://doi.org/10.1029/2006gc001309

Muxworthy, A. R., & McClelland, E. (2000). The causes of low-temperature demagnetization of remanence in multidomain magnetite. *Geophysical Journal International*, *140*(1), 115–131. https://doi.org/10.1046/j.1365-246x.2000.00000.x

Muxworthy, A. R., & Williams, W. (2006). Critical single-domain/multidomain grain sizes in noninteracting and interacting elongated magnetite particles: Implications for magnetosomes. *Journal of Geophysical Research*, *111*(B12), B12S12. https://doi.org/10.1029/2006JB004588

Muxworthy, A. R., Williams, W., & Virdee, D. (2003). Effect of magnetostatic interactions on the hysteresis parameters of single-domain and pseudo-single-domain grains. *Journal of Geophysical Research*, *108*(B11), 2517. https://doi.org/10.1029/2003jb002588

Nagy, L., Moreno, R., Muxworthy, A. R., Williams, W., Paterson, G. A., Tauxe, L., & Valdez-Grijalva, M. (2024). *Micromagnetic determination of the FORC response of paleomagnetically significant magnetite assemblages*. ESS Open Archive. https://doi.org/10.22541/essoar.170533987.78411398/v1

Nagy, L., Moreno, R., Williams, W., Paterson, G., Tauxe, L., & Muxworthy, A. R. (2024). Synth-forc. Retrieved from https://synth-forc.earthref.org/

Nagy, L., Williams, W., Muxworthy, A. R., Fabian, K., Almeida, T. P., Ó Conbhui, P., & Shcherbakov, V. P. (2017). Stability of equidimensional pseudo-single-domain magnetite over billion-year timescales. *Proceedings of the National Academy of Sciences*, *114*(39), 10356–10360. https://doi.org/10.1073/pnas.1708344114

Nagy, L., Williams, W., Tauxe, L., & Muxworthy, A. R. (2019). From nano to micro: Evolution of magnetic domain structures in multidomain magnetite. *Geochemistry, Geophysics, Geosystems*, *20*(6), 2907–2918. https://doi.org/10.1029/2019gc008319

Nagy, L., Williams, W., Tauxe, L., Muxworthy, A. R., & Ferreira, I. (2019). Thermomagnetic recording fidelity of nanometer-sized iron and implications for planetary magnetism. *Proceedings of the National Academy of Sciences of the United States of America*, *116*(6), 1984–1991. https://doi.org/10.1073/pnas.1810797116

Néel, L. (1949). Théorie du traînage magnétique des ferromagnétiques en grains fins avec applications aux terres cuites. *Annales de Geophysique*, *5*, 99–136.

Néel, L. (1955). Some theoretical aspects of rock-magnetism. *Advances in Physics*, *4*(14), 191–243. https://doi.org/10.1080/00018735500101204

Nikolaisen, E. S., Harrison, R. J., Fabian, K., & McEnroe, S. A. (2020). Hysteresis of natural magnetite ensembles: Micromagnetics of silicate-hosted magnetite inclusions based on focused-ion-beam nanotomography. *Geochemistry, Geophysics, Geosystems*, *21*(11), e2020GC009389. https://doi.org/10.1029/2020gc009389

Ó Conbhuí, P., Williams, W., Fabian, K., Ridley, P., Nagy, L., & Muxworthy, A. R. (2018). MERRILL: Micromagnetic Earth related robust interpreted language laboratory. *Geochemistry, Geophysics, Geosystems*, *19*(4), 1080–1106. https://doi.org/10.1002/2017gc007279

Özdemir, O., & Banerjee, S. K. (1982). A preliminary magnetic study of soil samples from west-central Minnesota. *Earth and Planetary Science Letters*, *59*(2), 393–403. https://doi.org/10.1016/0012-821x(82)90141-8

Özdemir, O., & Dunlop, D. J. (2014). Hysteresis and coercivity of hematite. *Journal of Geophysical Research-Solid Earth*, *119*(4), 2582–2594. https://doi.org/10.1002/2013jb010739

Paterson, G. A., Muxworthy, A. R., Yamamoto, Y., & Pan, Y. (2017). Bulk magnetic domain stability controls paleointensity fidelity. *Proceedings of the National Academy of Sciences*, *114*(50), 13120–13125. https://doi.org/10.1073/pnas.1714047114

Pauthenet, R., & Bochirol, L. (1951). Aimantation spontanee des ferrites. *Journal de Physique et le Radium*, *12*(3), 249–251. https://doi.org/10.1051/jphysrad:01951001203024900

Rave, W., Fabian, K., & Hubert, A. (1998). Magnetic states of small cubic particles with uniaxial anisotropy. *Journal of Magnetism and Magnetic Materials*, *190*(3), 332–348. https://doi.org/10.1016/S0304-8853(98)00328-X

Roberts, A. P., Almeida, T. P., Church, N. S., Harrison, R. J., Heslop, D., Li, Y., et al. (2017). Resolving the origin of pseudo-single domain magnetic behavior. *Journal of Geophysical Research-Solid Earth*, *122*(12), 9534–9558. https://doi.org/10.1002/2017jb014860

Roberts, A. P., Hu, P., Harrison, R. J., Heslop, D., Muxworthy, A. R., Oda, H., et al. (2019). Domain state diagnosis in rock magnetism: Evaluation of potential alternatives to the Day diagram. *Journal of Geophysical Research-Solid Earth*, *124*(6), 5286–5314. https://doi.org/10.1029/2018jb017049

Roberts, A. P., Pike, C. R., & Verosub, K. L. (2000). First-order reversal curve diagrams: A new tool for characterizing the magnetic properties of natural samples. *Journal of Geophysical Research*, *105*(B12), 28461–28475. https://doi.org/10.1029/2000jb900326

Roberts, A. P., Tauxe, L., Heslop, D., Zhao, X., & Jiang, Z. (2018). A critical appraisal of the "Day" diagram. *Journal of Geophysical Research-Solid Earth*, *123*(4), 2618–2644. https://doi.org/10.1002/2017jb015247

Shah, J., Williams, W., Almeida, T. P., Nagy, L., Muxworthy, A. R., Kovács, A., et al. (2018). The oldest magnetic record in our solar system identified using nanometric imaging and numerical modeling. *Nature Communications*, *9*(1), 1173. https://doi.org/10.1038/s41467-018-03613-1

Stoner, E. C., & Wohlfarth, E. P. (1948). A mechanism of magnetic hysteresis in heterogeneous alloys. *Philosophical Transactions of the Royal Society of London*, *240*(826), 599–642. https://doi.org/10.1098/rsta.1948.0007

Tauxe, L., Bertram, H. N., & Seberino, C. (2002). Physical interpretation of hysteresis loops: Micromagnetic modeling of fine particle magnetite. *Geochemistry, Geophysics, Geosystems*, *3*(10), 1–22. https://doi.org/10.1029/2001gc000241

Tauxe, L., Mullender, T. A. T., & Pick, T. (1996). Potbellies, wasp-waists, and superparamagnetism in magnetic hysteresis. *Journal of Geophysical Research*, *101*(B1), 571–583. https://doi.org/10.1029/95jb03041

15252027, 2024, 8, Downloaded from https://agupubs.onlinelibrary.wiley.com/doi/10.1029/2024GC011462 by Test, Wiley Online Library on [07/08/2024]. See the Terms and Conditions (https://onlinelibrary.wiley.com/terms-and-conditions) on Wiley Online Library for rules of use; OA articles are governed by the applicable Creative Commons License

Valdez-Grijalva, M. A., Muxworthy, A. R., Williams, W., Ó Conbhuí, P., Nagy, L., Roberts, A. P., & Heslop, D. (2018). Magnetic vortex effects on first-order reversal curve (FORC) diagrams for greigite dispersions. *Earth and Planetary Science Letters*, *501*, 103–111. https://doi.org/10.1016/j.epsl.2018.08.027

Valdez-Grijalva, M. A., Nagy, L., Muxworthy, A. R., Williams, W., Roberts, A. P., & Heslop, D. (2020). Micromagnetic simulations of first-order reversal curve (FORC) diagrams of framboidal greigite. *Geophysical Journal International*, *222*(2), 1126–1134. https://doi.org/10.1093/gji/ggaa241

Williams, W., & Dunlop, D. J. (1990). Some effects of grain shape and varying external magnetic-fields on the magnetic-structure of small grains of magnetite. *Physics of the Earth and Planetary Interiors*, *65*(1–2), 1–14. https://doi.org/10.1016/0031-9201(90)90070-E

Williams, W., & Dunlop, D. J. (1995). Simulation of magnetic hysteresis in pseudo-single-domain grains of magnetite. *Journal of Geophysical Research*, *100*(B3), 3859–3871. https://doi.org/10.1029/94jb02878

Williams, W., Fabian, K., Ridley, P., Nagy, L., Paterson, G., & Muxworthy, A. R. (2024). Merrill. Retrieved from https://bitbucket.org/wynwilliams/merrill

Williams, W., Muxworthy, A. R., & Paterson, G. A. (2006). Configurational anisotropy in single-domain and pseudosingle-domain grains of magnetite. *Journal of Geophysical Research*, *111*(B12), B12S13. https://doi.org/10.1029/2006jb004556

Williams, W., Paterson, G., & Nagy, L. (2024b). MERRILL micromagnetic modelling software version 1.8.6. *Zenodo*. https://doi.org/10.5281/zenodo.10556856

Zhao, G., Morvan, F., & Wan, X. (2014). Micromagnetic calculation for exchange-coupled nanocomposite permanent magnets. *Reviews in Nanoscience and Nanotechnology*, *3*(4), 227–258. https://doi.org/10.1166/rnn.2014.1058

15252027, 2024, 8, Downloaded from https://agupubs.onlinelibrary.wiley.com/doi/10.1029/2024GC011462 by Test, Wiley Online Library on [07/08/2024]. See the Terms and Conditions (https://onlinelibrary.wiley.com/terms-and-conditions) on Wiley Online Library for rules of use; OA articles are governed by the applicable Creative Commons License